

# Laser-induced quantum pumping in graphene

Pablo San-Jose,<sup>1</sup> Elsa Prada,<sup>2</sup> Henning Schomerus,<sup>3</sup> and Sigmund Kohler<sup>2</sup>

<sup>1)</sup>*Instituto de Estructura de la Materia (IEM-CSIC), Serrano 123, 28006 Madrid, Spain*

<sup>2)</sup>*Instituto de Ciencia de Materiales de Madrid, CSIC, Cantoblanco, 28049 Madrid, Spain*

<sup>3)</sup>*Department of Physics, Lancaster University, Lancaster, LA1 4YB, United Kingdom*

(Dated: 8 March 2013)

We investigate non-adiabatic electron pumping in graphene generated by laser irradiation with linear polarization parallel or perpendicular to the transport direction. Transport is dominated by the spatially asymmetric excitation of electrons from evanescent into propagating modes. For a laser with parallel polarization, the pumping response exhibits a subharmonic resonant enhancement which directly probes the Fermi energy; no such enhancement occurs for perpendicular polarization. The resonance mechanism relies on the chirality of charge carriers in graphene.

PACS numbers: 05.60.Gg, 73.40.Gk, 72.80.Vp, 72.40.+w

The periodic modulation of a mesoscopic conductor attached to electronic reservoirs can be used to induce a transfer of electrons across the system, which produces a dc current in absence of a bias voltage. Such *quantum pumps* can be driven adiabatically slowly, provided that their work cycle is oriented,<sup>1</sup> which requires variation of at least two parameters. For faster, non-adiabatic driving, single-parameter pumping is possible,<sup>2-4</sup> which has been observed in a number of experiments.<sup>5-11</sup>

With the advent of graphene, it has been suggested to exploit and probe the properties of this material both by adiabatic<sup>12-16</sup> and non-adiabatic pumping,<sup>17,18</sup> with the driving typically provided by applying ac electrostatic voltages. In this work, by contrast, we consider driving graphene by linearly polarized laser irradiation,<sup>19,20</sup> as is depicted in Fig. 1. We show that this results in a sizable pumped current, which moreover is resonantly enhanced when the polarization of the electric field is parallel with the transport direction. The resonance occurs at a Fermi energy equaling half the photon energy, and thus may be useful to characterize the properties of a graphene sample. The polarization dependence arises from a selection rule which directly probes the chirality of the charge carriers in graphene.

We consider a graphene monolayer sheet of length  $2L$

and width  $W$  connected to two highly doped leads, as shown in Fig. 1. In the absence of the laser irradiation, the potential energy in the sheet is  $U_B(x) = 0$ , while in the leads  $U_B(x) \ll 0$ ; the potential energy is independent of the transverse coordinate  $y$ . The low-energy excitations are then described by the quasi-one-dimensional Dirac Hamiltonian  $H_0 = \hbar v_F \mathbf{k} \cdot \boldsymbol{\sigma} + U_B(x)$ , where  $v_F \approx 10^6$  m/s denotes the Fermi velocity of graphene. The components of  $\boldsymbol{\sigma}$  are the Pauli matrices  $\sigma_x$  and  $\sigma_y$ , which act in a pseudo-spin space that physically describes the amplitudes on the two inequivalent lattice sites of graphene's honeycomb lattice. Because of the term  $\mathbf{k} \cdot \boldsymbol{\sigma}$  in  $H_0$ , the electronic states of graphene possess chirality, which is responsible for many of its properties,<sup>21</sup> including those that result in efficient pumping by ac gating.<sup>12,17</sup>

The pumping is induced by laser irradiation focused on a region of size  $L$  next to the left electrode, with linear polarization along the unit vector  $\mathbf{n}$  in the plane of the graphene sheet. The associated oscillating electric field  $\mathbf{E}(x, t) = E_0 \sin(\omega t) a(x) \mathbf{n}$  is modeled by a piecewise constant laser spot profile  $a(x)$  (the magnetic field in the graphene plane has a negligible physical effect). To avoid complications arising from a position-dependent scalar potential, we work with the Weyl gauge in which the electric field is derived from a time-dependent vector potential,  $\mathbf{E}(x, t) = -\partial \mathbf{A}(x, t) / \partial t$ . Using the minimal coupling  $\mathbf{k} \rightarrow \mathbf{k} + e\mathbf{A}$  for the electron charge  $-e$ , we obtain the time-dependent Dirac Hamiltonian

$$H(t) = H_0 + a(x) \cos(\omega t) U_{\mathbf{n}}, \quad (1)$$

where the constant coupling operator is given by

$$U_{\mathbf{n}} = ev_F \frac{E_0}{\omega} \mathbf{n} \cdot \boldsymbol{\sigma}. \quad (2)$$

It follows that the polarization direction  $\mathbf{n}$  couples to the pseudo-spin  $\boldsymbol{\sigma}$  and thus affects the quasiparticle chirality.

The pumped current can be obtained by Floquet scattering theory,<sup>22</sup> which is valid as long as interactions

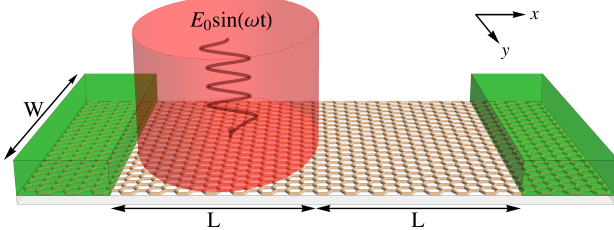


FIG. 1. Sketch of a graphene sheet of length  $2L$  and width  $W$  connected to two highly doped graphene leads. The left half of the sheet is driven periodically in time by laser irradiation of frequency  $\omega$  and amplitude  $E_0$ .

can be neglected. At low temperatures, the dc current is then given by the generalized Landauer formula<sup>2,23</sup>

$$I = \frac{4e}{h} \int_{-\infty}^{E_F} d\epsilon \Delta T(\epsilon), \quad (3)$$

where the factor 4 accounts for spin and valley degeneracy. The central quantity is the net transmission imbalance  $\Delta T(\epsilon) = \sum_n [T_{LR}^{(n)}(\epsilon) - T_{RL}^{(n)}(\epsilon)]$ , which involves the transmission coefficients  $T_{\ell\ell'}^{(n)}(\epsilon)$  from lead  $\ell = L, R$  to lead  $\ell' \neq \ell$ , where  $n$  labels sidebands reached by absorption or emission of  $n$  photons ( $n < 0$  corresponds to emission). The definition of the transmission coefficients includes the summation over the transverse wave number  $k_y$ , which here is conserved, and can be considered continuous for wide and short pumps ( $W \gg L$ ). The pumped current is non-zero since the specified setup is asymmetric. In particular, as in the case of driving by an ac gate voltage,<sup>12,17</sup> carriers entering the driving region from the left lead in evanescent modes can be promoted to propagating modes, which allows them to reach the right lead, while electrons arriving in evanescent modes from the right lead practically never reach the driven region; the result is net transport from left to right.

Before presenting quantitative results we establish the preferred pumping regime and the typical magnitude of the pumped current. There are two relevant parameters. The first is the effective driving strength

$$p = \left( \frac{|U_n|}{2\hbar\omega} \right)^2 = \left( \frac{ev_F E_0}{2\hbar\omega^2} \right)^2. \quad (4)$$

Adjacent sidebands possess relative energy shifts  $\hbar\omega$ , and are coupled by a “hopping” energy  $|U_n|/2$ . The ratio of these two quantities,  $\sqrt{p}$ , equals the number of sidebands that get populated in the scattering process,<sup>17</sup> i.e., the average number of absorbed or emitted photons. For  $p \ll 1$ , only one-photon processes play a practical role. Within the single-sideband approximation  $\Delta T$  is proportional to  $p$ , so that for small  $p$  the net transmission  $\Delta T/p$  is independent of driving strength  $|U_n|$ .

The second relevant parameter is the ratio  $\hbar\omega/E_L$  between the photon energy and the ballistic Thouless energy  $E_L = \hbar v_F/L$ , i.e., the energy scale associated with the length  $L$  of the driven region, with  $v_F$  the Fermi energy. This scale governs the formation of Fabry-Perot scattering resonances (different from the polarization-dependent resonance to be identified below), so that  $\hbar\omega/E_L$  provides a measure for the number of resonances within a window  $\hbar\omega$ . For  $\hbar\omega/E_L \gg 1$ , evanescent modes are densely spaced, which means that the quantum pumping mechanism by these modes is maximally efficient.<sup>17</sup>

We concentrate on the regime of universal and efficient quantum pumping of  $W \gg L$ ,  $p \ll 1$  and  $E_L \gg \hbar\omega$ . The pumped current (3) then becomes independent of  $L$ , and the response to the driving is proportional to the effective driving strength  $p$ , Eq. (4). Extracting this factor and

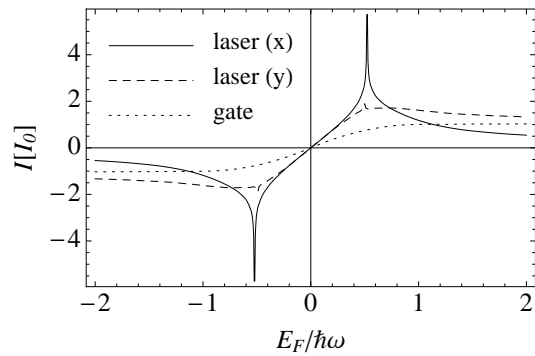


FIG. 2. Total current driven across a wide and short graphene pump, as a function of Fermi energy (measured from the Dirac point in the static sheet) for various driving mechanisms as indicated in the legend.

the scales of the energy and momentum integrals in the current formula, we obtain a characteristic current

$$I_0 = \frac{e}{h} \left( \frac{eE_0 v_F}{2\omega} \right)^2 \frac{W}{\hbar v_F}. \quad (5)$$

A laser in the visible red, with wavelength of  $\sim 850$  nm, 1 mW output power and  $1 \mu\text{m}$  spot size gives a typical coupling energy  $|U_n| = 0.1$  meV, and a photon energy  $\hbar\omega = 0.7$  eV. Hence  $p \approx 10^{-9}$ , and  $\hbar\omega/E_L \approx 2200$ , such that the conditions for efficient pumping are fulfilled. The characteristic current is then  $I_0 \sim 0.7$  nA. For a far infrared laser with a wavelength of  $50 \mu\text{m}$ , a power of 1 mW and a spot radius of  $50 \mu\text{m}$ , we have  $p \approx 7 \cdot 10^{-6}$  and  $\hbar\omega/E_L \approx 1900$ , and one may achieve much larger pumped currents of the order  $I_0 \sim 50$  nA.

The precise value of the pumped current can be obtained by wave matching of modes with fixed transverse momentum  $k_y$  and subsequent integration of the contributions of these modes. The resulting dependence on the Fermi energy (measured from the Dirac point in the static sheet) is shown in Fig. 2. As a consequence of particle-hole symmetry in the Dirac Hamiltonian, the pumped current is antisymmetry and vanishes at the Dirac point. Far from the Dirac point, i.e., for strongly doped graphene with  $|E_F| > \hbar\omega$ , the current saturates at a value of the order  $I_0$ . Thus, Eq. (5) indeed generally reflects the magnitude of the achievable pumped current. For a laser polarized in transport direction  $x$ , however, the pumped current displays a resonant feature at  $|E_F| = \hbar\omega/2$ , where  $I \gg I_0$ . The singularity is logarithmic and grows as the ratio  $\hbar\omega/E_L$  is increased. Circular polarization (not shown) produces a very similar resonant response. In contrast, for transverse polarization (along  $y$ ), we witness only a small hump, while driving by an ac gate voltage does not display any resonant features.<sup>17</sup>

This enhancement of the pumped current for  $x$  polarization arises from a resonant coupling between the pseudo-spin states at  $E_F = \pm\hbar\omega/2$ . This is revealed by inspecting the transmission imbalance  $\Delta T(\epsilon, k_y)$ , pre-

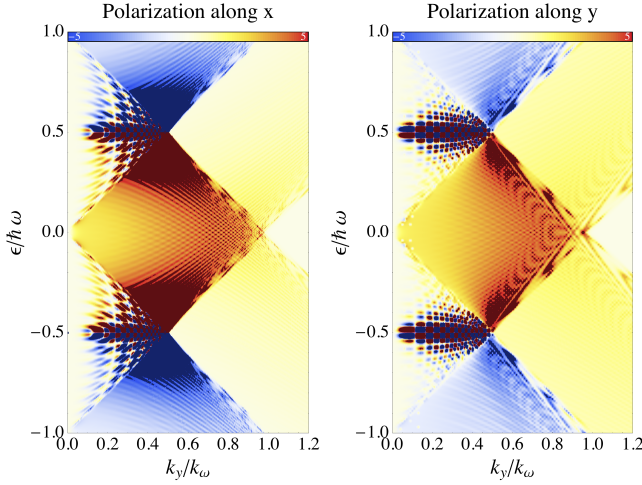


FIG. 3. Normalized net transmission  $\Delta T/p$ , with  $p \ll 1$  and  $\hbar\omega/E_L = 50$ , for laser-driven graphene with polarization in  $x$  (longitudinal) and  $y$  (transverse) directions. The transverse momentum is measured in units of  $k_\omega \equiv \hbar\omega/v_F$ . The color scale (top bar) corresponds to positive current (left to right) in red, and negative in blue.

sented in Fig. 3. A substantial pumping response is obtained in a diamond-shaped area, whose borders are defined by the transverse momenta at which modes in the sidebands  $n = 0, \pm 1$  turn from propagating to evanescent. This delineates the evanescent-mode pumping mechanism which also dominates the response to an ac gate voltage.<sup>12,17</sup> Notably, however, for laser driving a strong pumping response also arises from the subharmonic resonances at energies  $\epsilon \approx \pm \hbar\omega/2$ . These resonances extend into the range of propagating incoming electrons with  $\hbar v_F k_y < \epsilon$ . In the case of  $x$ -polarization the resonance evolves into a singular peak around the tips of the evanescent diamond, at  $v_F k_y = \omega/2$ .

This additional feature in the pumping response, which is absent for driving by ac gate voltages, reveals a fundamental feature of the coupling of laser fields to the chiral charge carriers in graphene. For fixed wavevector  $\mathbf{k}$ , the static Hamiltonian in the pump,  $H_0 = \hbar v_F \mathbf{k} \cdot \boldsymbol{\sigma}$ , possesses propagating eigenstates  $|\mathbf{k}, s\rangle$  with band index  $s = \pm 1$ , energies  $\epsilon_{\mathbf{k},s} = s \hbar v_F |\mathbf{k}|$  and pseudospin parallel to  $s\mathbf{k}$ . A laser with frequency  $\omega$  induces resonant transitions between any two such states with the same  $k_y$ , and energy difference  $|\epsilon_{\mathbf{k}_x k_y, s} - \epsilon_{\mathbf{k}'_x k_y, s'}| = \hbar\omega$ . The transition probability  $P = |\langle \mathbf{k}'_x, k_y, s' | \boldsymbol{\sigma} \cdot \mathbf{n} | \mathbf{k}_x, k_y, s \rangle|^2$  depends on the matrix element of the normalized driving operator  $U_n/|U_n| = \boldsymbol{\sigma} \cdot \mathbf{n}$ . This probability becomes maximal,  $P = 1$ , if  $\mathbf{k}, \mathbf{k}' \perp \mathbf{n}$ , and  $s\mathbf{k} = -s'\mathbf{k}$ . This resonant condition can be satisfied for  $\mathbf{n}$  in the  $x$ -direction, when  $v_F \mathbf{k} = (0, \omega/2)$  and  $s = -s'$ , which is manifested as a large pumping response at  $|\epsilon| \approx \hbar v_F k_y \approx \hbar\omega/2$  (see Fig. 3, left panel). The response around this point has a constant positive (negative) sign for  $|\epsilon|$  below (above)  $\hbar\omega/2$  and thus builds up to a large peak in the total cur-

rent. In contrast, for  $y$  polarization the response around  $\epsilon = \pm \hbar\omega/2$  oscillates as a function of  $k_y$ , which leads to a cancellation of different modes and a small overall contribution to the total pumped current.

In summary, driving graphene by laser irradiation can lead to a sizable pumped current, which furthermore is resonantly enhanced when the polarization is parallel to the transport direction. For lasers in the visible range, typical currents are  $I_0 = 0.7$  nA, while the resonant condition  $|E_F| = \hbar\omega/2$  corresponds to a relatively high doping, which may require chemical functionalization or liquid electrodes. Moreover, infrared lasers may be employed to lower the resonant condition to a much more accessible range of dopings ( $|E_F| \sim 12$  meV), while at the same time increasing  $I_0$  and suppressing possible inelastic effects due to electron-phonon interactions. The constraint in this case lies in keeping the laser spot size  $L$  below the mean free path in the flake.

This work was supported by the Spanish Ministry of Economy and Competitiveness through Grant Nos. FIS2008-00124/FIS (P.S.-J.), FIS2009-08744 (E.P.) and MAT2011-24331 (S.K.).

- <sup>1</sup>P. W. Brouwer, Phys. Rev. B **58**, R10135 (1998).
- <sup>2</sup>S. Kohler, J. Lehmann, and P. Hänggi, Phys. Rep. **406**, 379 (2005).
- <sup>3</sup>L. E. F. Torres, H. L. Calvo, C. G. Rocha, and G. Cuniberti, App. Phys. Lett. **99**, 092102 (2011).
- <sup>4</sup>Y. Zhou and M. W. Wu, arXiv:1206.3435 (2012).
- <sup>5</sup>T. H. Oosterkamp, T. Fujisawa, W. G. van der Wiel, K. Ishibashi, R. V. Hijman, S. Tarucha, and L. P. Kouwenhoven, Nature (London) **395**, 873 (1998).
- <sup>6</sup>M. D. Blumenthal, B. Kaestner, L. Li, S. Giblin, T. J. B. M. Janssen, M. Pepper, D. Anderson, G. Jones, and D. A. Ritchie, Nature Phys. **3**, 343 (2007).
- <sup>7</sup>L. DiCarlo, C. M. Marcus, and J. S. Harris, Jr., Phys. Rev. Lett. **91**, 246804 (2003).
- <sup>8</sup>B. Kaestner, V. Kashcheyevs, G. Hein, K. Pierz, U. Siegner, and H. W. Schumacher, Appl. Phys. Lett. **92**, 192106 (2008).
- <sup>9</sup>A. Fujiwara, K. Nishiguchi, and Y. Ono, Appl. Phys. Lett. **92**, 042102 (2008).
- <sup>10</sup>B. Kaestner, C. Leicht, V. Kashcheyevs, K. Pierz, U. Siegner, and H. W. Schumacher, Appl. Phys. Lett. **94**, 012106 (2009).
- <sup>11</sup>V. S. Khrapai, S. Ludwig, J. P. Kotthaus, H. P. Tranitz, and W. Wegscheider, Phys. Rev. Lett. **97**, 176803 (2006).
- <sup>12</sup>E. Prada, P. San-Jose, and H. Schomerus, Phys. Rev. B **80**, 245414 (2009).
- <sup>13</sup>G. M. M. Wakker and M. Blaauboer, Phys. Rev. B **82**, 205432 (2010).
- <sup>14</sup>M. Alos-Palop and M. Blaauboer, Phys. Rev. B **84**, 073402 (2011).
- <sup>15</sup>J.-F. Liu and K. S. Chan, Nanotechnology **22**, 395201 (2011).
- <sup>16</sup>T. Low, Y. Jiang, M. Katsnelson, and F. Guinea, Nano Lett. **12**, 850 (2012).
- <sup>17</sup>P. San-Jose, E. Prada, S. Kohler, and H. Schomerus, Phys. Rev. B **84**, 155408 (2011).
- <sup>18</sup>T. Kaur, L. Arrachea, and N. Sandler, ArXiv:1203.3952 [cond-mat].
- <sup>19</sup>H. L. Calvo, H. M. Pastawski, S. Roche, and L. E. F. F. Torres, App. Phys. Lett. **98**, 232103 (2011).
- <sup>20</sup>Z. Gu, H. A. Fertig, D. P. Arovas, and A. Auerbach, Phys. Rev. Lett. **107**, 216601 (2011).
- <sup>21</sup>A. H. Castro Neto, F. Guinea, N. M. R. Peres, K. S. Novoselov, and A. K. Geim, Rev. Mod. Phys. **81**, 109 (2009).
- <sup>22</sup>M. Moskalets and M. Büttiker, Phys. Rev. B **66**, 205320 (2002).
- <sup>23</sup>M. Wagner and F. Sols, Phys. Rev. Lett. **83**, 4377 (1999).